Investigation of erosion-corrosion behavior of (WTi)C based weld overlays

Islam, Md. Aminul; Jiang, Jiaren (Jimmy); Xie, Yongsong; Fiala, Petr

Publisher's version / Version de l'éditeur:
https://doi.org/10.1016/j.wear.2017.07.016
Wear, 390-391, pp. 155-165, 2017-07-29

Investigation of erosion-corrosion behavior of (WTi)C based weld overlays

Md. Aminul Islam [a], Jiaren (Jimmy) Jiang [a], Yongsong Xie [a], Petr Fiala [b]

[a] *National Research Council Canada*
Mining Wear and Corrosion Laboratory
Vancouver, BC, Canada V6T 1W5

[b] *Oerlikon Metco*
10108 114 St, Fort Saskatchewan,
AB, Canada T8L 4R1

Abstract

Erosion-corrosion is responsible for severe damage and high maintenance costs in many industrial operations involving slurry handling such as oil sands and mineral processing. While tungsten carbide reinforced Ni-based alloy overlays are frequently used for applications requiring extremely high wear resistance, they tend to suffer from extensive carbide degradation during the weld cladding process which has been shown to severely impair their erosion-corrosion resistance. Recently, new (WTi)C based overlays are being developed to alleviate some of the limitations associated with the nickel-based tungsten carbide overlays. In this study, three different overlays reinforced with (WTi)C and one tungsten carbide were assessed using a slurry pot erosion-corrosion testing apparatus where the total erosion-corrosion (E-C) rate as well as the separate components of synergistic effect was determined. Erosion-corrosion test was performed at 30°C, in an aqueous slurry containing 35wt.% AFS 50-70 silica sand and 3.5wt% NaCl. A special SEM technique was employed to examine changes on the specimen surface at specific overlay locations before and after erosion-corrosion test in order to identify the effect of corrosion on erosion and vice-versa. It was found that tungsten is more prone to dissolution in the matrix during the welding process than titanium, which forms W-depletion/Ti-rich layer around the (WTi)C particle. Dissolution of tungsten and titanium promotes the formation of secondary carbides in the matrix. Erosion-

corrosion performance of the overlays largely depends on increased fraction of retained primary (WTi)C phase.

Key words: Erosion-corrosion, synergistic effect, overlays, slurry pot, (WTi)C

1 Introduction

Extreme wear and corrosive environment in the mineral and oil sands industries decreases the productivity and useful life of the equipment. The combined action of erosion and corrosion due to the presence of sand/mineral particles flowing in a corrosive fluid produces a high degradation rate of the hydrotransport equipment. Material loss rate due to combined erosion-corrosion is usually significantly higher than the sum of material loss rate due to pure erosion and pure corrosion acting separately [1]–[4]. Hence, materials subjected to erosion-corrosion processes must be able to resist mechanical and electrochemical degradation due to erosive particle impact in a corrosive medium [5], [6].

Erosion-corrosion damage of critical areas in the slurry handling equipment can be minimized by the application of protective overlays [7]–[9]. The erosion resistance of weld overlays is achieved due to the combination of matrix toughness and hardness of the reinforcing particles [10]–[12]. It also depends on the volume fraction, size and distribution of the hard phases [10], [13], [14]. On the other hand, erosion-corrosion is a complex phenomenon and erosion-corrosion resistance not only depends on the reinforcing particles, but also the matrix composition and carbide matrix interface [13], [15]–[18].

Tungsten carbides (WC or WC/W_2C eutectoid) in a self-fluxing Ni-based alloy are widely used () in the oil sands/mineral industry to provide protection in low stress sliding abrasion, slurry abrasion and erosion-corrosion conditions [15], [19]–[21]. They combine high hardness, good wettability to the matrix and low thermal expansion coefficient [22], [23]. However, during deposition, thermal decomposition of carbides can occur due to interaction with lower melting point matrix constituent

[17], [20]. Dissolution of the carbides results in reduced wear performance of the deposit [16], [24]–[26]. In addition, dissolved carbides lead to the formation of brittle secondary phases which may be detrimental to the wear resistance of the deposit [27]. It was found that spherical and angular cast tungsten carbides (WC/W_2C) are more affected by carbide dissolution than monocrystalline tungsten carbides [28], [29].

To alleviate the issue of carbide degradation associated with the nickel-based tungsten carbide overlays, MMC overlays reinforced with other types of carbides such as (WTi)C are being explored. In this study, the erosion-corrosion behavior of three (WTi)C based overlays and one monocrystalline WC overlay has been studied using a slurry pot erosion-corrosion test apparatus at 30°C, in an aqueous slurry containing 35wt.% AFS 50-70 silica sand and 3.5wt% NaCl.

2 Experimental

2.1 Test materials and characterization

Four plasma transferred arc weld overlays were studied. Their nominal compositions, hardness, carbide type and volume fraction of large (primary) carbides are listed in Table 1. It is important to note that measured carbide volume fraction (vol%) only included the original undissolved (primary) carbide particles. The 50 wt% (WTi)C-316L-Si overlay had considerably lower primary carbide volume fraction after welding than the nominal value.

Table 1 Test materials and basic characteristics.

Material	Carbide type	Powder		Overlay	
		Carbide wt%	Carbide vol%	(*)Measured carbide vol%	Hardness (HRC)
50 wt% (WTi)C/ 316L-Si (Fe17Cr12Ni2.5Mo2Si)	(W, Ti)C	50	44.3	14.4	44.5 ± 1.9
60 wt% (WTi)C/ 316L-Si (Fe17Cr12Ni2.5Mo2Si)	(W, Ti)C	60	54.4	37.1	59.4 ± 1.6
60 wt% (WTi)C/ MC625 (Ni22Cr9Mo4Nb4Fe)	(W, Ti)C	60	56.4	40.1	55.3 ± 2.0
Plasmadur 51322 (60 wt% WC/ Ni7Cr4Si2Fe1.5B)	WC	60	44.7	46.1	51.3 ± 1.5

* Only the original un-dissolved carbide particles were included in the "Measured carbide vol%".

2.2 Slurry pot erosion-corrosion (SPEC) testing

Erosion-corrosion test was conducted on a slurry pot erosion-corrosion tester. The setup of the tester is shown in Figure 1. The unit consists of a 4-litre glass vessel to hold the slurry, a neoprene-lined impeller that is rotated to impel the slurry against the test surfaces, a heating/cooling system (chiller) and a three-electrode cell with a Gamry PC4/750 potentiostat to allow for electrochemical assessment and cathodic protection control. Electrochemical tests were conducted in-situ vs. saturated calomel electrode (SCE) and Pt counter electrode. The test conditions for erosion-corrosion assessment are shown in Table 2. In order to discern any preferential damage under various test conditions, surface examination was performed using a Hitachi S-3500N scanning electron microscope (SEM) of specific phases in the overlay before and after each test at the same locations.

Table 2 **Slurry pot erosion-corrosion (SPEC) test parameters.**

Slurry	35wt% AFS 50-70 silica sand + 3.5wt% NaCl in water
Impeller speed	900 rpm
Slurry temperature	30°C
Test duration	6 hr
Environment	Open air

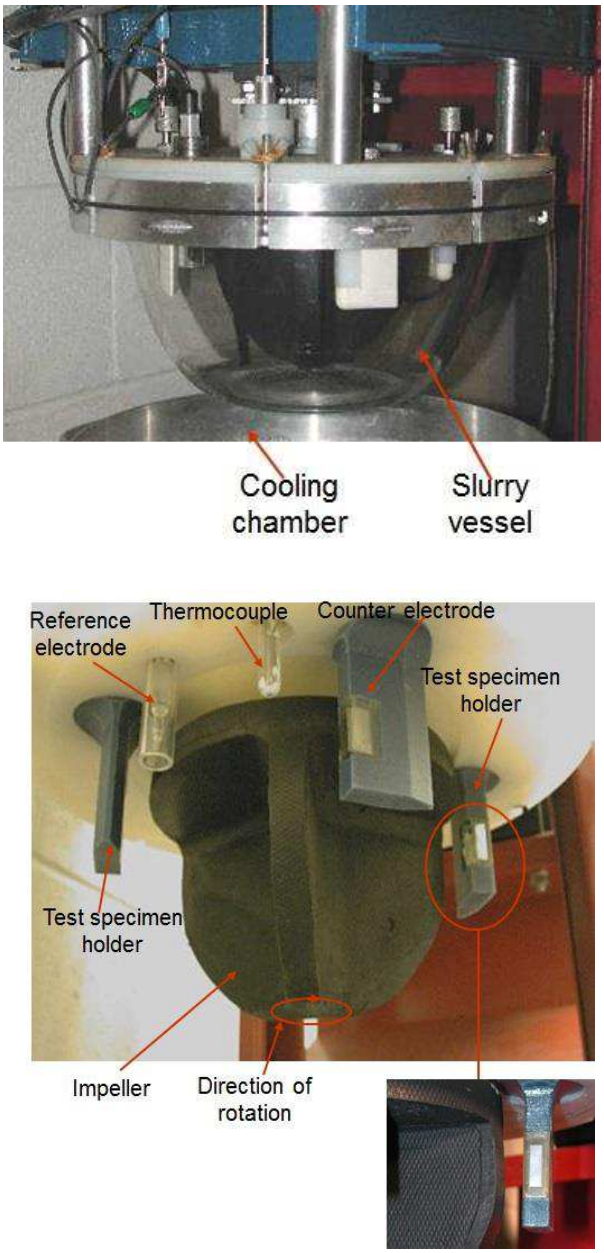

Figure 1 **The slurry pot erosion-corrosion (SPEC) tester setup.**

2.3 Specimen preparation

The specimen dimensions are 18±0.5 mm x 6±0.5 mm x 5±0.5 mm, where 18 mm x 6 mm is the test surface which constitutes a test area of 1.08 cm^2. All surfaces adjacent to the test surface are ground perpendicular to each other. The testing surface is polished to 1 µm diamond suspension prior to the experiments. All specimens are mounted in epoxy, leaving only the test surface exposed to the testing environment. An electrical contact is attached to the specimen requiring electrochemical assessment/control before embedding in epoxy.

2.4 Assessment of erosion-corrosion synergy

The erosion-corrosion synergy is determined/analyzed according to the ASTM G119-04 standard guide [30]. The total material loss under erosion-corrosion (E-C) conditions, *Kec*, is related to the synergistic component, *Ks*, by Eq. 1

$$K_{ec} = K_{eo} + K_{co} + K_s \quad \text{.....} \quad (1)$$

Where, K_{ec} = total E-C rate, K_{eo} = erosion-only material loss rate (erosion in the absence of corrosion), K_{co} = corrosion-only material loss rate (corrosion in the absence of erosion), and K_s = synergy.

The total material loss rate, *Kec*, can also be divided into the following components as expressed in Eq. 2:

$$K_{ec} = (K_{eo} + \Delta K_e) + (K_{co} + \Delta K_c) = Ke + Kc \quad \text{.....} \quad (2)$$

Where, K_e = total erosion rate, K_c = total corrosion rate, ΔK_e = corrosion-enhanced erosion, and ΔK_c = erosion-enhanced corrosion. Eq. 2 provides more detailed information on key contributors to E-C loss. From Eq. 1 & Eq. 2, the erosion-corrosion synergy and its various components can be calculated/expressed by:

$$K_s = \Delta K_e + \Delta K_c = K_{ec} - (K_{eo} + K_{co}) \quad \text{.....} \quad (3)$$

$$\Delta K_c = K_c - K_{co} \quad \text{.....} \quad (4)$$

$\Delta K_e = K_s - \Delta K_c$ ..... (5)

Total erosion-corrosion rate, *Kec*, is measured by mass loss using a microbalance with a reading accuracy of 0.01 mg. The erosion-only rate, *Keo*, is also determined by measuring the mass loss following testing in the same slurry but with the specimen being cathodically protected. The total corrosion rate in the presence of erosion, *Kc*, and the corrosion-only rate in the absence of erosion, *Kco*, are determined using the polarization resistance technique [31]. These are measured in the slurry pot erosion-corrosion test system with the rotator running with and without sand, respectively. From these measured values of material loss rate, the synergistic effect, *Ks*, the erosion-enhanced corrosion, ΔK_c, and the corrosion-enhanced erosion, ΔK_e, can be obtained according to Eq. 3, Eq. 4 and Eq. 5, respectively.

All the material loss rates are expressed in $cm^3/h/cm^2$.

3 Results and discussion

3.1 Microstructural characterization of overlays

The overlay microstructure is diverse and a single SEM micrograph is not representative of overall overlay microstructure. Figure 2 shows the SEM micrograph of 50wt% (WTi)C/316L-Si at different magnifications. Carbide distribution is relatively uniform but the volume fraction is much lower (14.4 vol%) than the nominal amount (50wt% is equivalent to about 44 vol%). A significant amount of eutectic (tungsten-rich) microstructure or networks of carbides was observed along the grain boundaries in the matrix. EDS line scan on 50wt% (WTi)C/ 316L-Si indicates that tungsten (W) in the (WTi)C is more prone to dissolution than titanium (Ti) in the matrix, forming a W-depletd/Ti-rich carbide layer around (WTi)C particle/matrix interface (Figure 3 (a)). The matrix has been modified by dissolved (WTi)C (Figure 3 (b)). The eutectic has typical morphologies for Fe-W-C alloys: Austenite + $(W, Fe)_6C$. Dissolved Ti precipitates as small (WTi)C. Due to higher dissolution of W from (WTi)C, there is enough W in the matrix to form WC.

In the 60wt% (WTi)C/ 316L-Si overlay, the matrix has two types of characteristic microstructures: regions containing fine white particles and regions free from such particles (Figure 4). This is mainly due to the relative movement of the PTA torch and the workpiece (oscillation speed and the transverse speed). As a result some material re-melts and has a longer molten state (more time to dissolve (WTi)C and form precipitates). The fine particle dense region contains blocky white carbides, gray-colored blocky phases and eutectic W-rich structures as shown in Figure 4 (b). Matrix in the particle sparse region has networks of gray-colored precipitates only (Figure 4 (c), (d)). Figure 5 shows EDS mapping of 60wt% (WTi)C/ 316L-Si. The white phases in the matrix are tungsten carbides (WC) and the gray particles (blocky or dendritic) are (WTi)Cs. Some Cr carbides are also formed in the matrix.

60wt% (WTi)C/ MC625 also has two typical regions in the matrix as shown in Figure 6 (a). In the dense fine particle region, the fine precipitates have different morphologies, including blocky white carbides (Figure 6 (c)), gray-colored globular phases and white dendrites (Figure 6 (b)). Thick W-depleted surface layer was also observed around primary carbide.

On the other hand, in the Plasmadur 51322 overlay, the microstructure is uniform across the specimen surface with minimal carbide degradation (Figure 7). Small amount of (W, Cr) carbides (η phase) are formed along grain boundaries in the matrix.

Minimal carbide (macrocrystalline WC) degradation in Plasmadur 51322 as compared to Metco overlays (cast (WTi)C) is mainly because; Plasmadur 51322 contain Ni self-fluxing alloy as matrix. It has lower melting temperature and low viscosity to produce better welds. Metco-clad 316L-Si (MC 316L-Si) and Metco-clad 625 (MC625) were designed as stand-alone alloys and do not have as low viscosity as Ni self-fluxing alloys. Combined with a lower density of (WTi)C particles, it is more difficult for these particles to penetrate the weld pool. Some (WTi)C particles bounce off and results in the lower measured carbide content. In addition, PTA

deposition parameters, Fe matrix and a high Cr content further decrease the content of the primary carbides in Metco overlays.

Because of its high dissolution rate, WC cannot be used in Fe matrix (MC 316L-Si, MC625) and matrix containing high Cr. Plasmadur 51322 matrix contains low Cr and most of its Cr is tied in carbides and does not contribute to corrosion resistance. On the other hand, MC 316L-Si and MC625 contain relatively higher Cr (as evident from EDS mapping) and provide better corrosion resistance. It is believed that, if macrocrystalline WC is used in MC 316L-Si or MC625 matrix, it will provide much inferior results compared to (WTi)C.

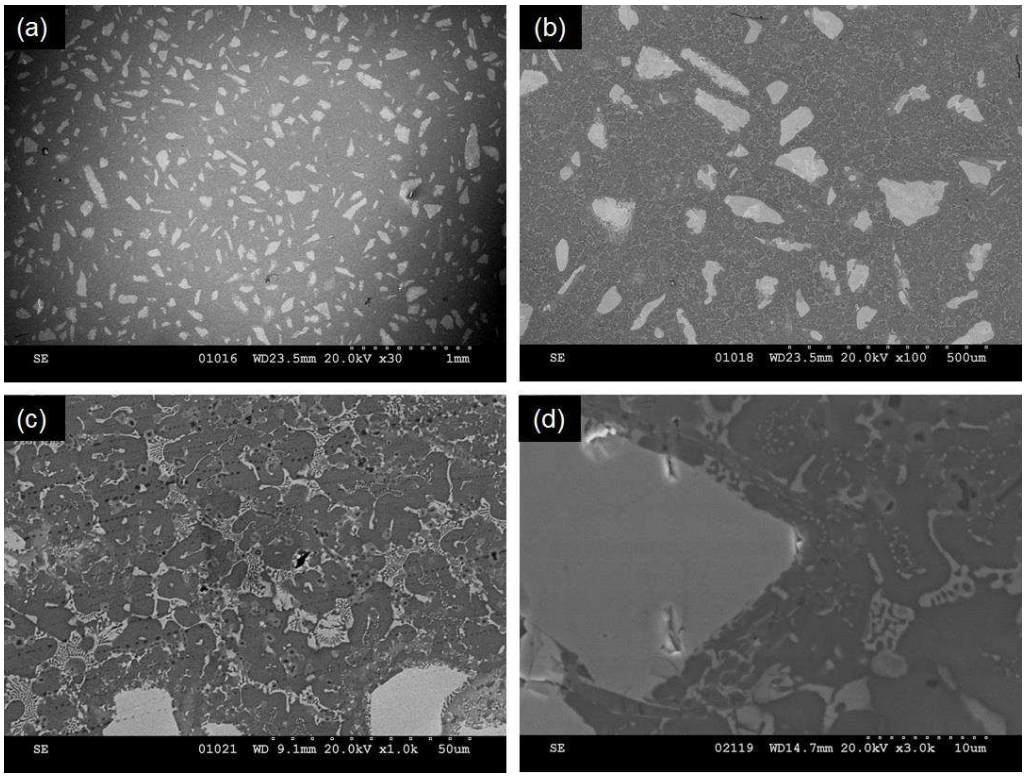

Figure 2 SEM micrograph of 50wt% (WTi)C/ 316L-Si.

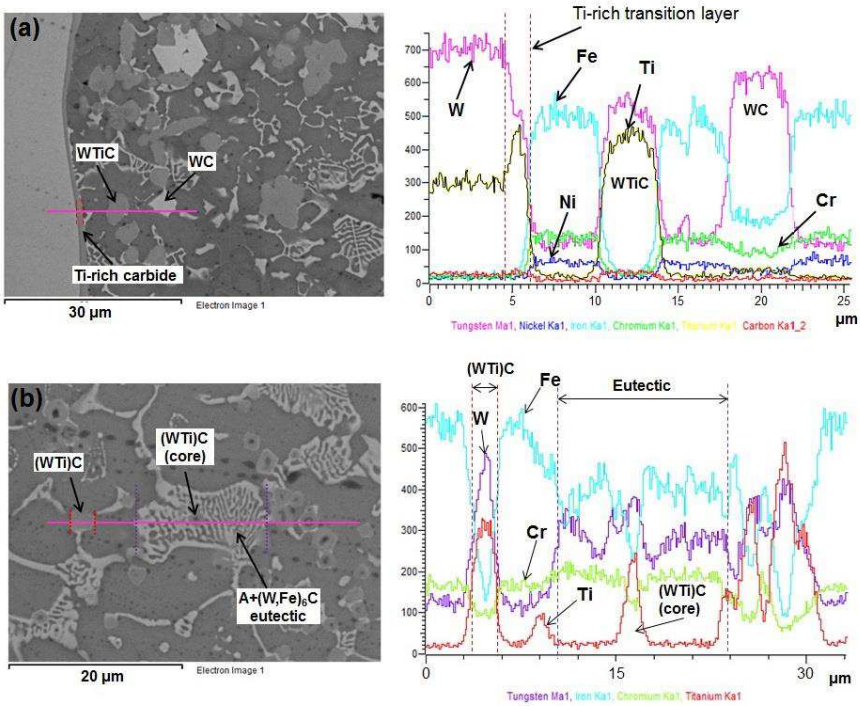

Figure 3 EDS line scan on 50wt% (WTi)C/ 316L-Si.

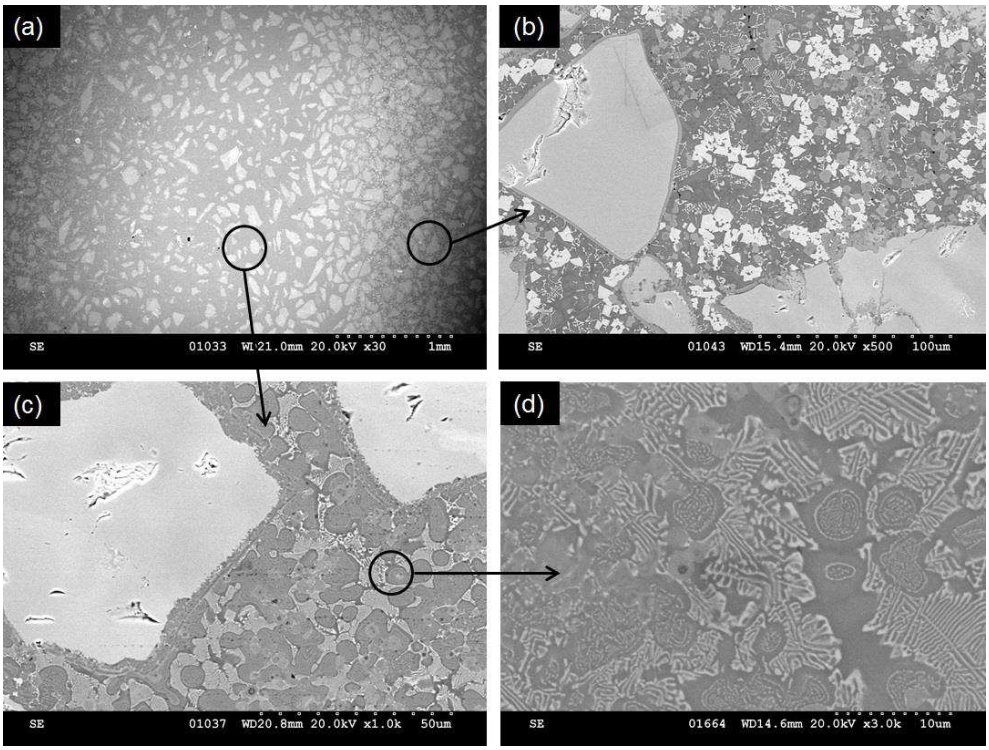

Figure 4 SEM micrograph of 60wt% (WTi)C/ 316L-Si.

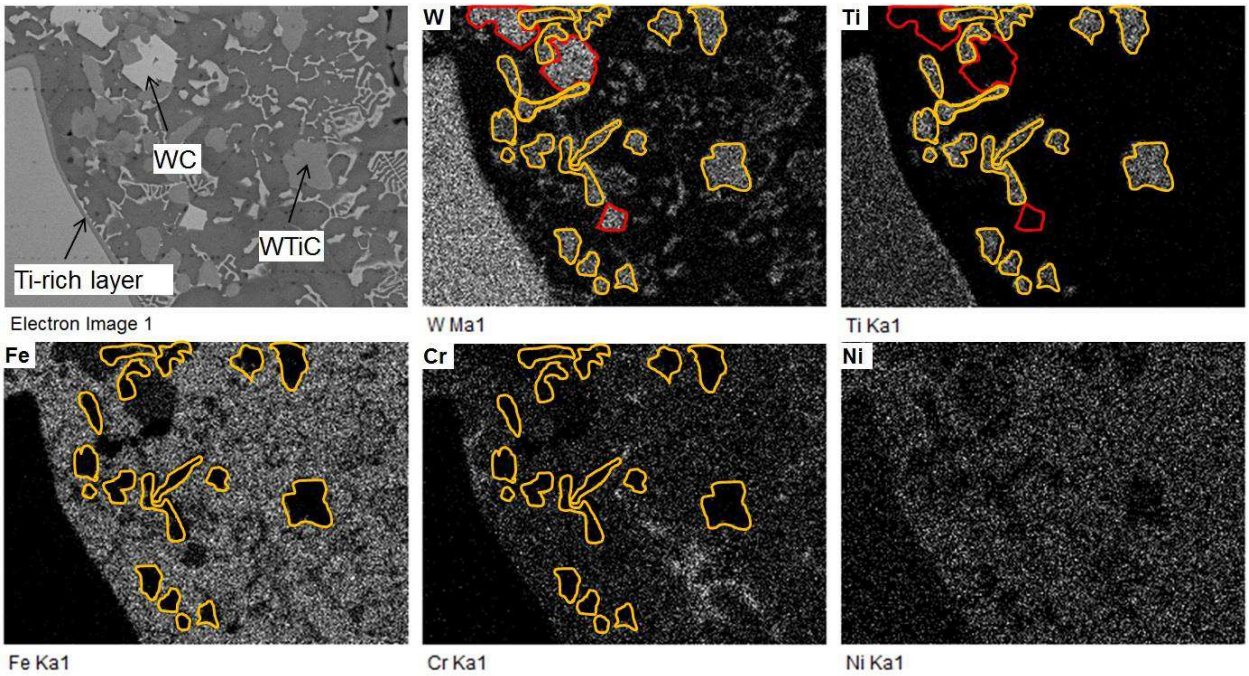

Figure 5 EDS mapping of 60wt% (WTi)C/ 316L-Si.

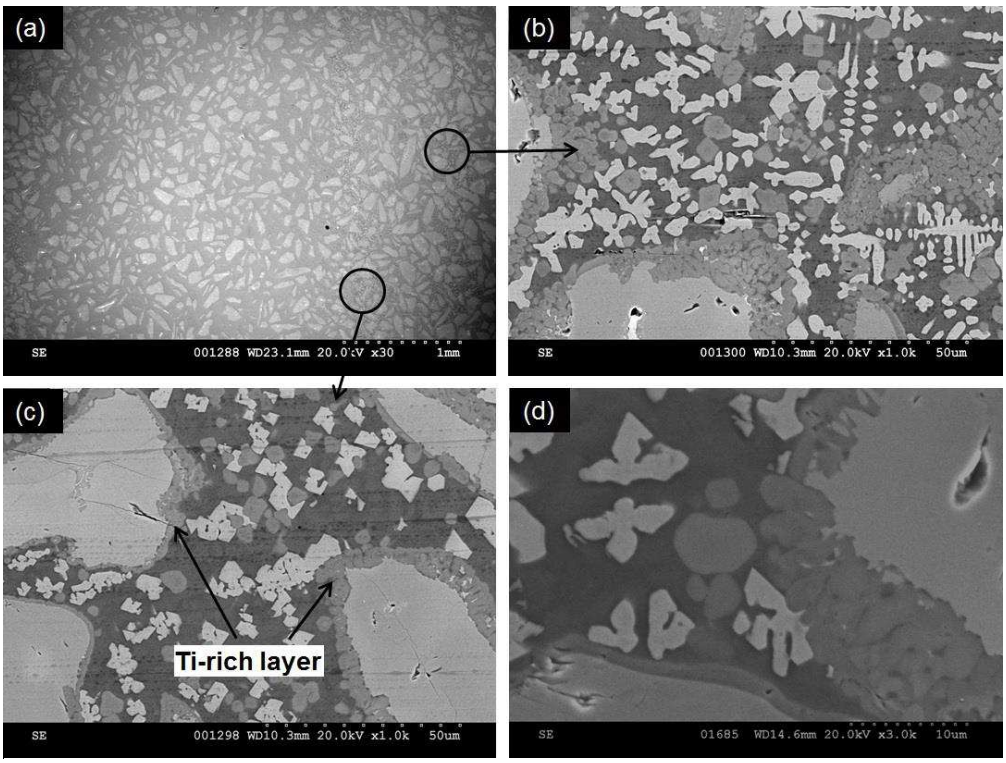

Figure 6 SEM micrograph of 60wt% (WTi)C/ MC625.

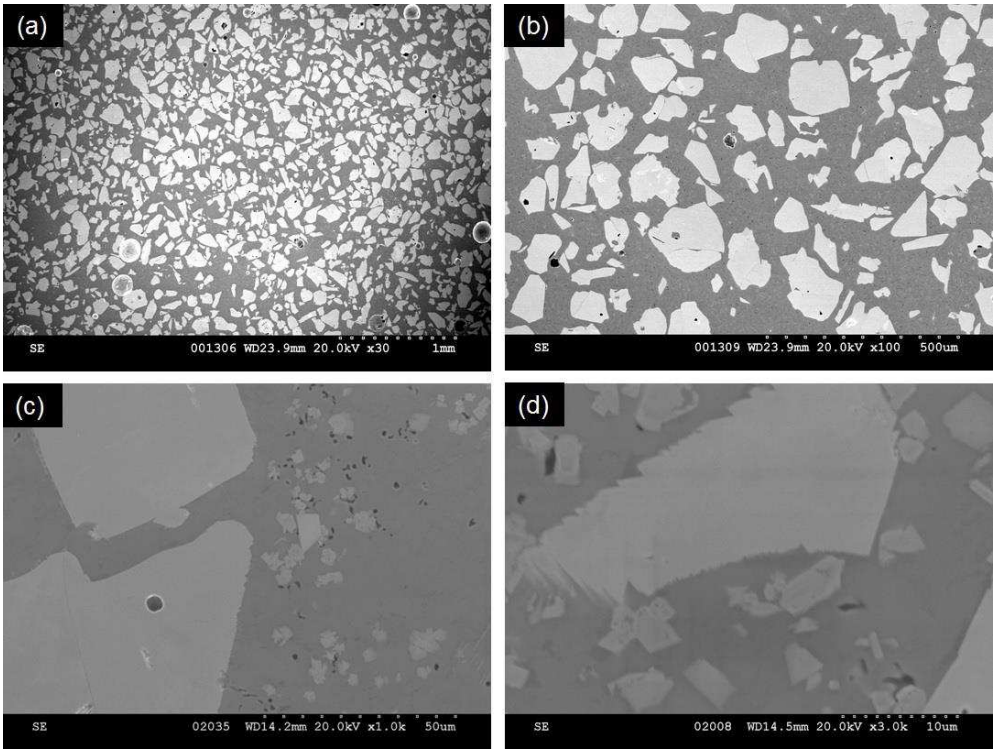

Figure 7 SEM micrograph of Plasmadur 51322.

3.2 Erosion-corrosion results

Figure 8 (a) shows the material loss rate due to erosion-corrosion, erosion only, corrosion only and synergy of the four evaluated overlays. Plasmadur 51322 has the highest erosion and erosion-corrosion resistance as compared with other overlays. This can probably be partially attributed to the higher undissolved carbide vol% in this overlay [32]–[36]. The erosion-corrosion resistance of Plasmadur 51322 and the 60wt% (WTi)C/ MC625 overlays is better than two versions of tungsten carbide overlays evaluated previously in this lab under the same testing conditions [1]: (a) 50 vol% of mixed tungsten carbide in NiBSi matrix (Kec = 7.35×10^{-5}) where the carbide particles are composed of crushed eutectic (WC/W_2C), spherical eutectic (WC/W_2C) and macrocrystalline WC particles and (b) Macro WC/NiCrBSi overlay (Kec = 1.8×10^{-5}) containing 50 vol% macrocrystalline WC. The contribution of pure corrosion rate to overall material loss rate is small for all the overlays.

Figure 8 (b) shows the material loss rate due to synergy and the contribution from erosion-enhanced corrosion and corrosion-enhanced erosion. It is interesting to note that erosion-enhanced corrosion (ΔKc) dominates the synergistic effect, Ks, for all overlays. 60wt% (WTi)C/316L overlay displayed much higher corrosion-enhanced erosion (42%) as compared with the other overlays.

Figure 9 shows the comparison of wear surface of 50wt% (WTi)C/316L-Si overlay at two locations before (Figure 9 (a) and (c)) and after (Figure 9 (b) and (d)) erosion-only test. Uniform erosion occurred in the matrix after pure erosion. The degradation of large (W,Ti)C particles was by brittle fracture as indicated by the solid red circles in Figure 9 (a) – (d). It is interesting to note that pre-existing surface cracks and porosity did not show significant influence on the overall erosion process as shown in Figure 9 (a) and (b) (dotted yellow circles). Figure 10 and Figure 11 show the SEM micrographs of changes in erosion surfaces of 60wt% (WTi)C/316L-Si and Plasmadur 51322 after pure erosion, respectively. The pull-out of some small (W,Ti)C carbide particles and brittle fracture of large (W,Ti)C particles were observed, but no apparent evidence of corrosion along the carbide/ matrix interface could be identified (Figure 10 (a) and (b)). Large and small monocrystalline WC particles underwent comparatively less degradation during the pure erosion (Figure 11).

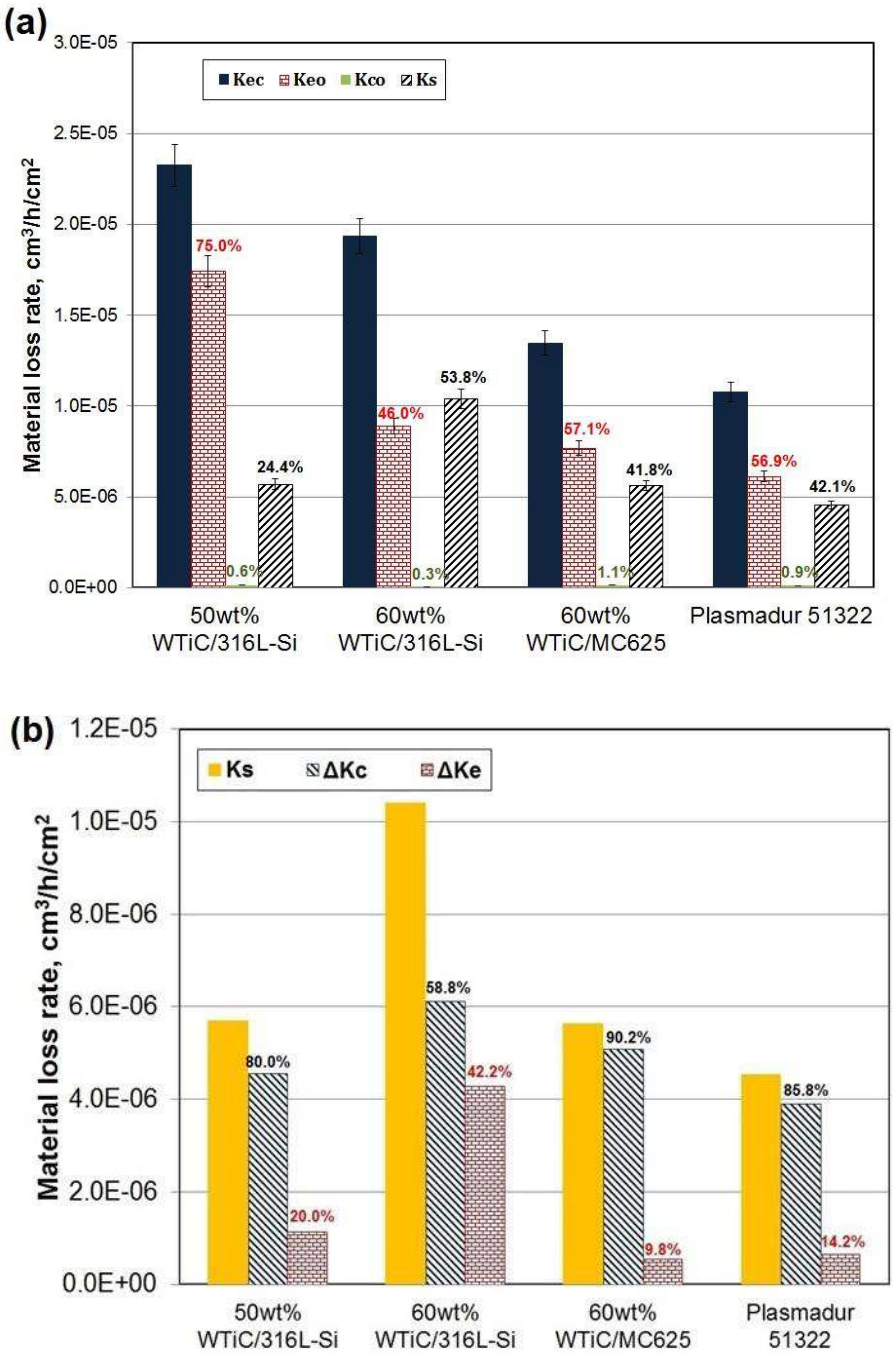

Figure 8 Erosion-corrosion synergy analysis of the overlays.

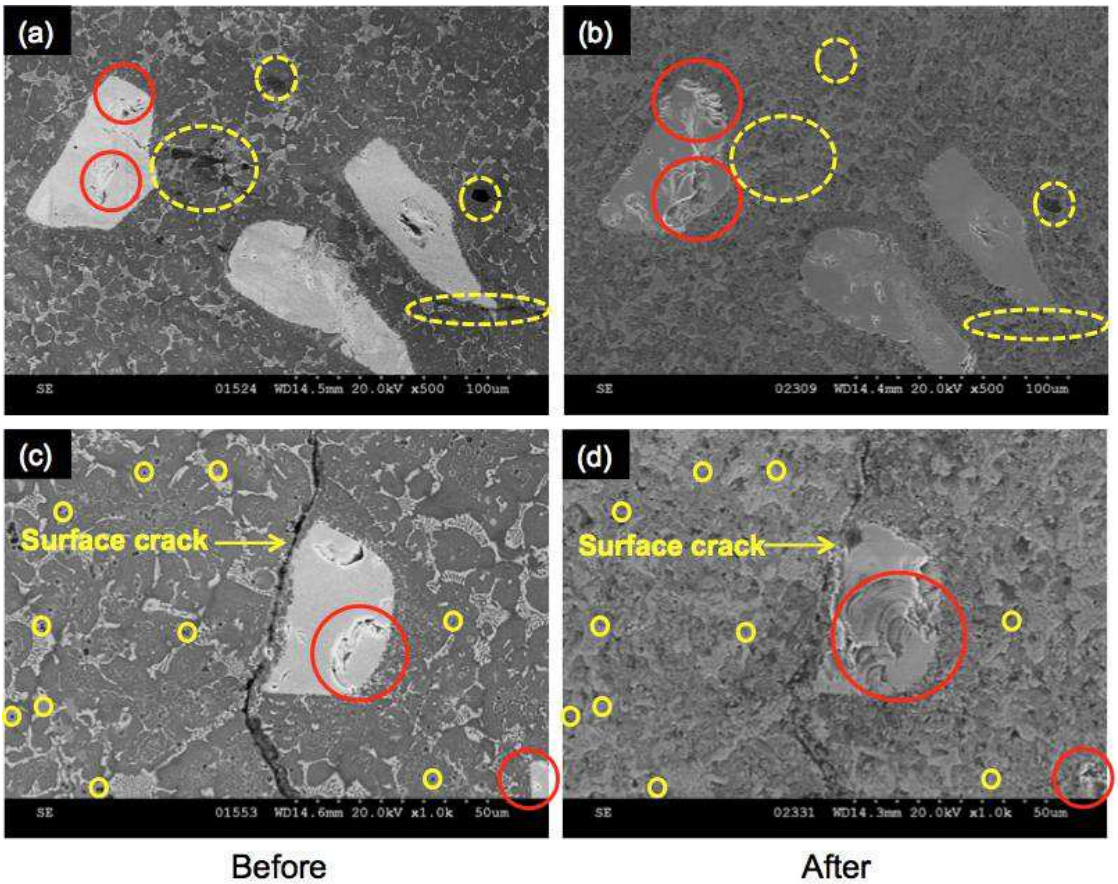

Figure 9 Comparison of wear surfaces of the 50wt% (WTi)C/316L-Si overlay before and after erosion-only test: (a) & (c) two separate locations on the surface before test; and (b) and (d) the corresponding locations at (a) and (c) after the erosion-only test. (a)-(d) degradation of large (W,Ti)C particles by brittle fracture (solid red circle), (a)-(b) pre-existing surface crack and porosity does not show significant influence on erosion (dotted yellow circle).

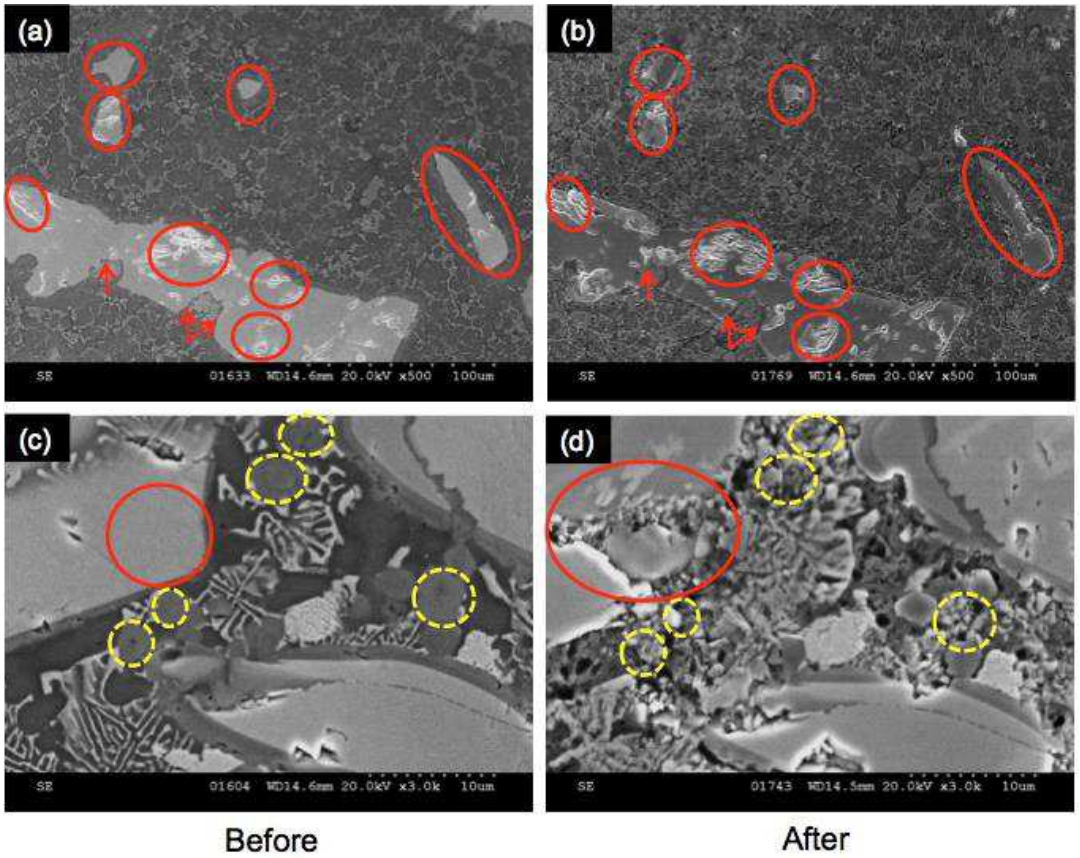

Figure 10 SEM micrograph of 60wt% (WTi)C/316L-Si after erosion only. (a)-(d) brittle fracture of (W,Ti)C particles (solid red circle), (a)-(b) no evidence of corrosion along the carbide/ matrix interface (red arrow), which illustrates the effectiveness of cathodic protection, (c)-(d) small (W,Ti)C pull out (dotted yellow circle).

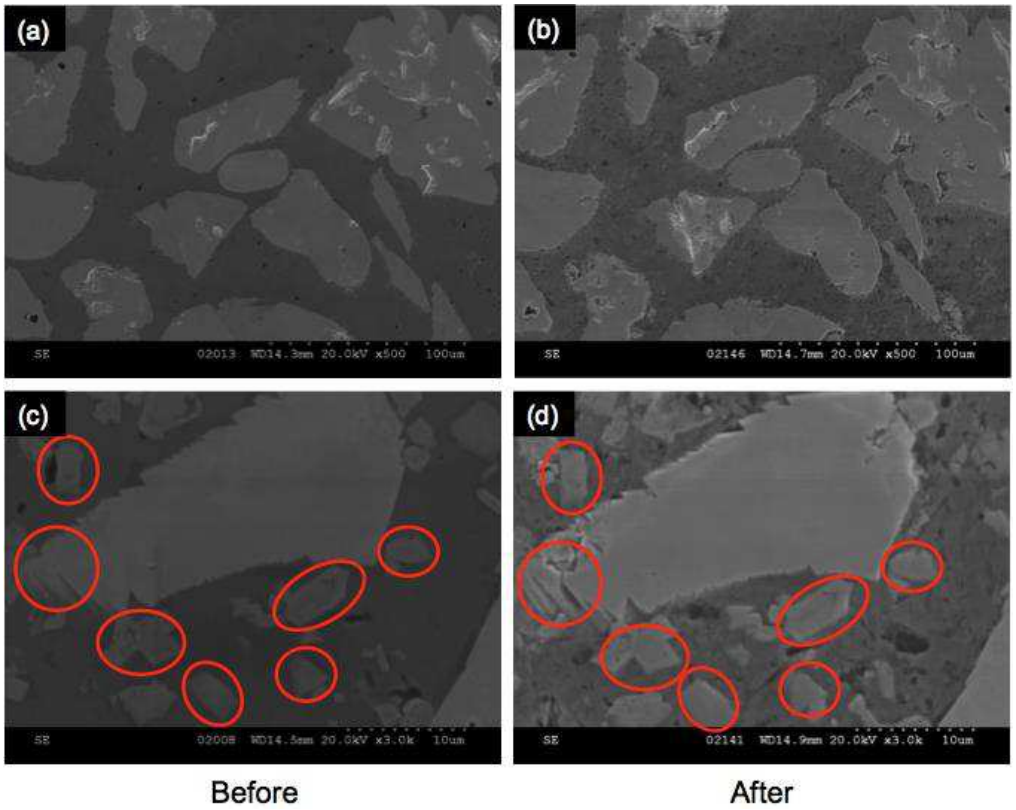

Figure 11 **SEM micrograph of Plasmadur 51322 after pure erosion. (a)-(d) less degradation of large and small monocrystalline WC than large and small (WTi)C.**

Figure 12 shows the comparison of wear surface changes before and after erosion-corrosion test for the 60wt% (WTi)C/316L-Si overlay. Clearly, erosion-corrosion caused more severe damage than in erosion-only test (Figure 10). Smaller (W,Ti)C particles were more easily removed, offering less erosion-corrosion resistance, as compared with larger ones. It is believed that preferential corrosion along the (W, Ti)C/matrix interface can accelerate the removal of small (W,Ti)C particles from the matrix, causing corrosion-enhanced erosion, which can be evidently seen by comparing Figure 12 (c) and (d).

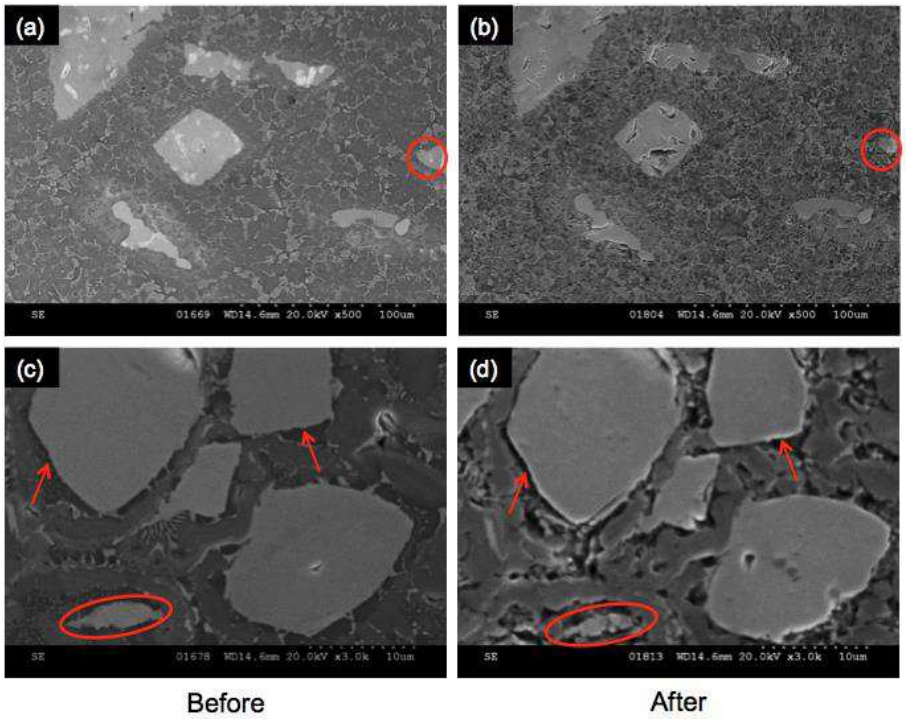

Figure 12 **SEM micrograph of 60wt% (WTi)C/316L-Si after erosion-corrosion. (a)-(d) severe damage of small (WTi)C particle, (c)-(d) preferential corrosion along the (WTi)C/matrix interface (red arrow).**

For the 50wt% (WTi)C/316L-Si overlay, extensive degradation of the primary (WTi)C particles occurred during the deposition process. The measured volume fraction of un-dissolved carbide (14 vol%) particles was much lower than the nominal value (44 vol%), Table 1. As has been presented earlier, tungsten is more prone to dissolution than titanium in the matrix. As a result, a W-depletion/Ti-rich carbide layer around (WTi)C particle/matrix interface is created. The dissolved W and Ti produce small (WTi)C precipitates and eutectic microstructure in the matrix. These W rich eutectic and small (WTi)C particles offer less erosion protection as compared with large (WTi)C particles (Figure 9). Thus, the 50wt% (WTi)C/316L-Si overlay exhibited inferior erosion and erosion-corrosion resistance due to the much lower amount of undissolved primary carbide. On the other hand, minimal carbide degradation was observed in the Plasmadur 51322 overlay which showed better erosion and erosion-corrosion resistance than the three (WTi)C based overlays.

4 Conclusions

In this study, four metal matrix composite (MMC) weld overlays were assessed using a slurry pot erosion-corrosion tester. These materials included three (W, Ti)C reinforced overlays and one monocrystalline WC based overlay, Plasmadur 51322. Total erosion-corrosion rate and separate components of synergistic effect were determined. The following conclusions can be made from the current work:

1. Under the erosion-only conditions, Plasmadur 51322 has the highest erosion resistance.
2. (WTi)C/316L-Si matrix overlays display inferior erosion-corrosion resistance to that of the (WTi)C/MC625 matrix overlay.
3. Higher volume fraction of undissolved (large primary) carbide provides better erosion-corrosion resistance.
4. Although total erosion-corrosion material loss rate for 50wt% (WTi)C/316L-Si is higher than 60wt% (WTi)C/316L-Si, it has much lower synergistic effect.
5. The contribution of pure corrosion rate to overall material loss rate is very small for all the studied overlays.
6. The synergistic effect, Ks, was dominated by erosion-enhanced corrosion (ΔKc) for all the evaluated overlays.
7. Large carbide particles offer better erosion protection than the fine W-rich eutectic and (WTi)C precipitates formed in the matrix from dissolved carbides during welding.
8. Preferential corrosion along the (WTi)C / matrix interface weakens the matrix support and accelerates the removal (pull-out) of small (WTi)C particles from the matrix, causing corrosion-enhanced erosion.

Acknowledgements

The authors would like to express their gratitude to the members of the NRC/Industry Mining Wear Materials Research Consortium for their support.

References

[1] M. Jones and R. J. Llewellyn, "Erosion-corrosion assessment of tungsten carbide-based plasma-tranferred arc-welded overlays," *Corros. J. Sci. Eng.*, vol. 68, no. 2, pp. 26001–26003, 2012.

[2] S. Zhou, M. M. Stack, and R. C. Newman, "Characterization of Synergistic Effects Between Erosion and Corrosion in an Aqueous Environment Using Electrochemical Techniques," *Corrosion*, vol. 52, no. 12, pp. 934–946, Dec. 1996.

[3] M. A. Islam and Z. N. Farhat, "Mechanical and Electrochemical Synergism of API X42 Pipeline Steel During Erosion-Corrosion," *J. Bio- Tribo-Corrosion*, vol. 1, no. 4, pp. 1–18, 2015.

[4] M. A. Islam, Z. N. Farhat, E. M. Ahmed, and A. Alfantazi, "Erosion enhanced corrosion and corrosion enhanced erosion of API X70 pipeline steel," *Wear*, vol. 302, no. 1–2, pp. 1592–1601, 2013.

[5] A. Neville, F. Reza, S. Chiovelli, and T. Revega, "Assessing Metal Matrix Composites for Corrosion and Erosion-Corrosion Applications in the Oil Sands Industry," *Corrosion*, vol. 62, no. 8, pp. 657–675, Aug. 2006.

[6] E. J. J. Wentzel and C. Allen, "Erosion-corrosion resistance of tungsten carbide hard metals with different binder compositions," *Wear*, vol. 181–183, no. PART 1, pp. 63–69, Feb. 1995.

[7] T. Liyanage, G. Fisher, and A. P. Gerlich, "Microstructures and abrasive wear performance of PTAW deposited Ni-WC overlays using different Ni-alloy chemistries," *Wear*, vol. 274–275, pp. 345–354, 2012.

[8] J. F. Flores, A. Neville, N. Kapur, and A. Gnanavelu, "Erosion-corrosion degradation mechanisms of Fe-Cr-C and WC-Fe-Cr-C PTA overlays in concentrated slurries," *Wear*, vol. 267, no. 11, pp. 1811–1820, 2009.

[9] H. Wang, W. Xia, and Y. Jin, "A study on abrasive resistance of Ni-based coatings with a WC hard phase," *Wear*, vol. 195, no. 1–2, pp. 47–52, Jul. 1996.

[10] R. L. Deuis, J. M. Yellup, and C. Subramanian, "Metal-matrix composite coatings by PTA surfacing," *Compos. Sci. Technol.*, vol. 58, no. 2, pp. 299–309, Jan. 1998.

[11] M. Kirchgaßner, E. Badisch, and F. Franek, "Behaviour of iron-based hardfacing alloys under abrasion and impact," *Wear*, vol. 265, no. 5–6, pp. 772–779, 2008.

[12] M. F. Buchely, J. C. Gutierrez, L. M. Leon, and A. Toro, "The effect of microstructure on abrasive wear of hardfacing alloys," *Wear*, vol. 259, no. 1–6, pp. 52–61, 2005.

[13] J. Przybylowicz and J. Kusinski, "Structure of laser cladded tungsten carbide

composite coatings," *J. Mater. Process. Technol.*, vol. 109, no. 1–2, pp. 154–160, 2001.

[14] R. Llewellyn and C. Tuite, "Hardfacing fights wear in oil sands operation," *Weld. J.*, vol. 74, no. 3, 1995.

[15] S. W. Huang, M. Samandi, and M. Brandt, "Abrasive wear performance and microstructure of laser clad WC/Ni layers," *Wear*, vol. 256, no. 11–12, pp. 1095–1105, 2004.

[16] M. Jones and U. Waag, "The influence of carbide dissolution on the erosion-corrosion properties of cast tungsten carbide/Ni-based PTAW overlays," *Wear*, vol. 271, no. 9–10, pp. 1314–1324, 2011.

[17] S. Ilo, C. Just, E. Badisch, J. Wosik, and H. Danninger, "Effects of interface formation kinetics on the microstructural properties of wear-resistant metal–matrix composites," *Mater. Sci. Eng. A*, vol. 527, no. 23, pp. 6378–6385, 2010.

[18] H. Liao, B. Normand, and C. Coddet, "Influence of coating microstructure on the abrasive wear resistance of WC/Co cermet coatings," *Surf. Coatings Technol.*, vol. 124, no. 2, pp. 235–242, 2000.

[19] A. Neville, F. Reza, S. Chiovelli, and T. Revega, "Erosion-corrosion behaviour of WC-based MMCs in liquid-solid slurries," *Wear*, vol. 259, no. 1–6, pp. 181–195, 2005.

[20] M. Anderson, S. Chiovelli, and D. Reid, "Wear-Resistant Materials for Use in the Oil Sands Hydraulic Transportation Process," *Mater. Resour. Recover. Transp. Metall. Soc. CIM*, pp. 451–465, 1998.

[21] P. Wu, H. M. Du, X. L. Chen, Z. Q. Li, H. L. Bai, and E. Y. Jiang, "Influence of WC particle behavior on the wear resistance properties of Ni-WC composite coatings," *Wear*, vol. 257, no. 1–2, pp. 142–147, 2004.

[22] V. A. de Souza and A. Neville, "Corrosion and erosion damage mechanisms during erosion–corrosion of WC–Co–Cr cermet coatings," *Wear*, vol. 255, no. 1, pp. 146–156, 2003.

[23] A. Neville, F. Reza, S. Chiovelli, and T. Revega, "Erosion–corrosion behaviour of WC-based MMCs in liquid–solid slurries," *Wear*, vol. 259, no. 1, pp. 181–195, 2005.

[24] A. Klimpel, A. Lisiecki, A. S. Klimpel, and A. Rzeźnikiewicz, "Robotized GMA surfacing of cermetal deposits," *J. Achiev. Mater. Manuf. Eng.*, vol. 18, no. 1–2, pp. 395–398, 2006.

[25] G. Fisher, T. Wolfe, and K. Meszaros, "The effects of carbide characteristics on the performance of tungsten carbide-based composite overlays, deposited by plasma-transferred arc welding," *J. Therm. Spray Technol.*, vol. 22, no. 5, pp. 764–771, 2013.

[26] J. Nurminen, J. Näkki, and P. Vuoristo, "Microstructure and properties of hard and wear resistant MMC coatings deposited by laser cladding," *Int. J. Refract. Met. Hard Mater.*, vol. 27, no. 2, pp. 472–478, 2009.

[27] J. F. Flores, A. Neville, N. Kapur, and A. Gnanavelu, "An experimental study of the erosion-corrosion behavior of plasma transferred arc MMCs," *Wear*, vol. 267, no. 1–4, pp. 213–222, 2009.

[28] D. Harper, M. Gill, K. W. D. Hart, and M. Anderson, "Plasma transferred arc overlays reduce operating costs in oil sands processing," *Proc. Int. Therm. Spray*, pp. 278–283, 2002.
[29] R. C. Gassmann, "Laser cladding with (WC+ W2C)/Co–Cr–C and (WC+ W2C)/Ni–B–Si composites for enhanced abrasive wear resistance," *Mater. Sci. Technol.*, vol. 12, no. 8, pp. 691–696, 1996.
[30] B. Madsen, "Standard guide for determining amount of synergism between wear and corrosion," *ASTM Int.*, vol. G119–09, pp. 1–7, 1994.
[31] ASTM, "Standard test method for conducting potentiodynamic polarization resistance measurements," *ASTM Int.*, vol. G59–97, pp. 1–4, 2014.
[32] S. G. Sapate and A. . Rama Rao, "Effect of carbide volume fraction on erosive wear behaviour of hardfacing cast irons," *Wear*, vol. 256, no. 7, pp. 774–786, 2004.
[33] R. Zhou, Y. Jiang, and D. Lu, "The effect of volume fraction of WC particles on erosion resistance of WC reinforced iron matrix surface composites," *Wear*, vol. 255, no. 1, pp. 134–138, 2003.
[34] J. K. Fulcher, T. H. Kosel, and N. F. Fiore, "The effect of carbide volume fraction on the low stress abrasion resistance of high Cr-Mo white cast irons," *Wear*, vol. 84, no. 3, pp. 313–325, Feb. 1983.
[35] R. J. Llewellyn, S. K. Yick, and K. F. Dolman, "Scouring erosion resistance of metallic materials used in slurry pump service," *Wear*, vol. 256, no. 6, pp. 592–599, Mar. 2004.
[36] A. N. J. Stevenson and I. . Hutchings, "Wear of hardfacing white cast irons by solid particle erosion," *Wear*, vol. 186–187, pp. 150–158, Jul. 1995.